How to cite: *Angew. Chem. Int. Ed.* **2023**, *62*, e202308761
doi.org/10.1002/anie.202308761

Catalytic Nanomedicine

Liposomal Enzyme Nanoreactors Based on Nanoconfinement for Efficient Antitumor Therapy

Ran Wang[+], Yingjie Yu[+], Meiyu Gai, Ana Mateos-Maroto, Svenja Morsbach, Xiang Xia, Maomao He, Jiangli Fan, Xiaojun Peng, Katharina Landfester, Shuai Jiang,* and Wen Sun**

Abstract: Enzymatic reactions can consume endogenous nutrients of tumors and produce cytotoxic species and are therefore promising tools for treating malignant tumors. Inspired by nature where enzymes are compartmentalized in membranes to achieve high reaction efficiency and separate biological processes with the environment, we develop liposomal nanoreactors that can perform enzymatic cascade reactions in the aqueous nanoconfinement of liposomes. The nanoreactors effectively inhibited tumor growth in vivo by consuming tumor nutrients (glucose and oxygen) and producing highly cytotoxic hydroxyl radicals (•OH). Co-compartmentalization of glucose oxidase (GOx) and horseradish peroxidase (HRP) in liposomes could increase local concentration of the intermediate product hydrogen peroxide (H_2O_2) as well as the acidity due to the generation of gluconic acid by GOx. Both H_2O_2 and acidity accelerate the second-step reaction by HRP, hence improving the overall efficiency of the cascade reaction. The biomimetic compartmentalization of enzymatic tandem reactions in biocompatible liposomes provides a promising direction for developing catalytic nanomedicines in antitumor therapy.

Introduction

Enzymes play an indispensable role in biological reactions and metabolic processes by reducing the activation energy and significantly increasing the rate of chemical reactions. Cascade reactions involving multiple enzymes are the basis for signal transmission and metabolism (e.g., oxidative phosphorylation) in living organisms.[1] In eukaryotic cells, the enzymes are compartmentalized in specific organelles and biomolecular condensates, which provide a confined environment for multi-step reactions in order to accomplish desired biological processes with high reaction efficiency and independency.[2]

Most research has focused on mimicking nature's compartmentalization strategy with synthetic systems.[3] Various artificial cellular and subcellular analogs, e.g., artificial cells and nano-organelles, were developed to mimic the basic cell structure and reactions.[4] This compartmentalization not only retains enzymatic function, but allows assembling the target enzymes with a high degree of control to mimic complex natural catalytic processes.[5] However, quantitative compartmentalization of defined enzyme combinations to achieve spatiotemporal control over cascade reactions remains challenging. Using these synthetic systems for real biomedical applications has been rarely achieved.

Due to their unique capsular configuration, hollow nanocontainers are suitable biomimetic encapsulation systems (i.e., having a large internal reservoir for cargo loading surrounded by a solid shell that protects the cargo).[6] Hollow silica nanocontainers were often used to encapsulate enzymes because of their good mechanical stability and high porosity, which allows diffusion of reaction substrates and products across the shell.[7] Enzymes are preferably loaded in the interior of nanocontainers. However, in situ enzyme encapsulation during silica formation requires harsh synthetic conditions (e.g., using ammonia solutions as catalyst or cationic surfactants as templates), which are deleterious for enzymatic activity.[8] Polymersomes are another alternative for entrapping enzymes in enzymatic nanoreactors, in their aqueous core.[9] In this case, the synthesis of block copolymers requires multi-step process.[10] Moreover, the biocompatibility of synthetic polymers remains a major issue for in vivo applications.[11] In addition, giant unilamellar

[*] R. Wang,[+] X. Xia, M. He, Prof. J. Fan, Prof. X. Peng, Prof. W. Sun
State Key Laboratory of Fine Chemicals, Frontiers Science Center for Smart Materials Oriented Chemical Engineering, Dalian University of Technology
2 Linggong Road, Hi-tech Zone, Dalian 116024 (China)
E-mail: sunwen@dlut.edu.cn

Y. Yu,[+] Prof. S. Jiang
Key Laboratory of Marine Drugs, Chinese Ministry of Education, School of Medicine and Pharmacy, Ocean University of China
Qingdao 266003 (China)
E-mail: jiangshuai@ouc.edu.cn

Dr. M. Gai, Dr. A. Mateos-Maroto, Dr. S. Morsbach, Prof. K. Landfester
Max Planck Institute for Polymer Research
Ackermannweg 10, 55128 Mainz (Germany)
E-mail: landfester@mpip-mainz.mpg.de

Prof. J. Fan, Prof. W. Sun
Ningbo Institute of Dalian University of Technology
No. 26 Yucai Road, Jiangbei District, Ningbo 315016 (China)

[+] These authors contributed equally to this work.

vesicles (GUVs) and giant endoplasmic reticulum vesicles (GERVs), with growth fusion and cell-like mechanical/chemical properties, are widely used as artificial cell models for the encapsulation of biomacromolecules.[12] However, due to their large size (usually >1000 nm), the long diffusion distance of glucose is not conducive for the enzymatic reaction. More importantly, the produced reactive oxygen species (ROS) show a short lifetime, thus a long diffusion distance of ROS would result in inefficient damage to external biomolecules. In comparison, liposome have been widely applied in clinical practice due to their good biocompatibility and suitable size.[13] Liposome drugs are primarily administered intravenously. Numerous studies have demonstrated that liposome drugs can accumulate at sites of enhanced vascular permeability in vivo through enhanced permeability and retention (EPR) effect, making it promising for targeted antitumor therapy.

In this study, we developed liposome-based enzymatic nanoreactors (LNRs) mimicking the structure and tandem reactions of eukaryotic organelles for antitumor therapy (Scheme 1). Both glucose oxidase (GOx) and horseradish peroxidase (HRP) were co-loaded in the liposomes aqueous core. Although there are already couples of reports about using GOx and HRP to perform cascade reactions in different carrier systems like mesoporous silica or metal-organic framework (MOF).[14] However, as aforementioned the harsh synthesis conditions and multi-step synthesis route not only make the operation of these nanocapsules difficult, but also lower the enzyme activity. In contrast, the co-compartmentalization of both enzymes in liposomes increases the overall tandem reaction efficiency. The GOx in nanoreactors can consume the glucose in tumor cells to produce gluconic acid and hydrogen peroxide (H_2O_2). The lower pH level achieved by the produced gluconic acid and the increase in local H_2O_2 concentration can accelerate HRP's catalytic efficiency, resulting in the production of highly cytotoxic hydroxyl radicals (•OH), which kills tumor cells. The enzymatic LNRs showed good biocompatibility and efficient antitumor efficacy in vitro and in vivo. Hence, the biomimetic nanoreactors combining the good biocompatibility of liposomes with the high efficiency of enzymatic reactions provides a promising candidate for catalytic nanomedicines in antitumor therapy.

Results and Discussion

Preparation of Liposomal Nanoreactors

In this study, the LNRs were prepared by thin-film dispersion and extrusion. L-α-phosphatidylcholine (egg PC), cholesterol (Chol), and 1,2-dioleoyl-sn-glycero-3-phosphoethanolamine (DOPE) were used to prepare the liposomes. These phospholipids have been used in commercial liposome formulations with proved biosafety, which is promising for biomedical applications. During the hydration process, different enzymes (none, GOx, HRP, and GOx/HRP) were added to prepare various kinds of LNRs formulation (Empty-LNRs, GOx-LNRs, HRP-LNRs, and GOx/HRP-LNRs). Enzymes remained active after encapsulation and were accessible for external reactants. As shown in cryo-Transmission electron microscopy (cryo-TEM) image, the microscopic morphology of liposomes showed spherical-like vesicles with a narrow size distribution (PDI = 0.13, Figure 1a). LNRs lipid bilayer could both prevent enzyme leakage and allow the diffusion of reactive species. As shown in Table 1, the hydrodynamic radius (R_h) of LNRs showed the same increasing trend (61 nm vs. 69 nm) after

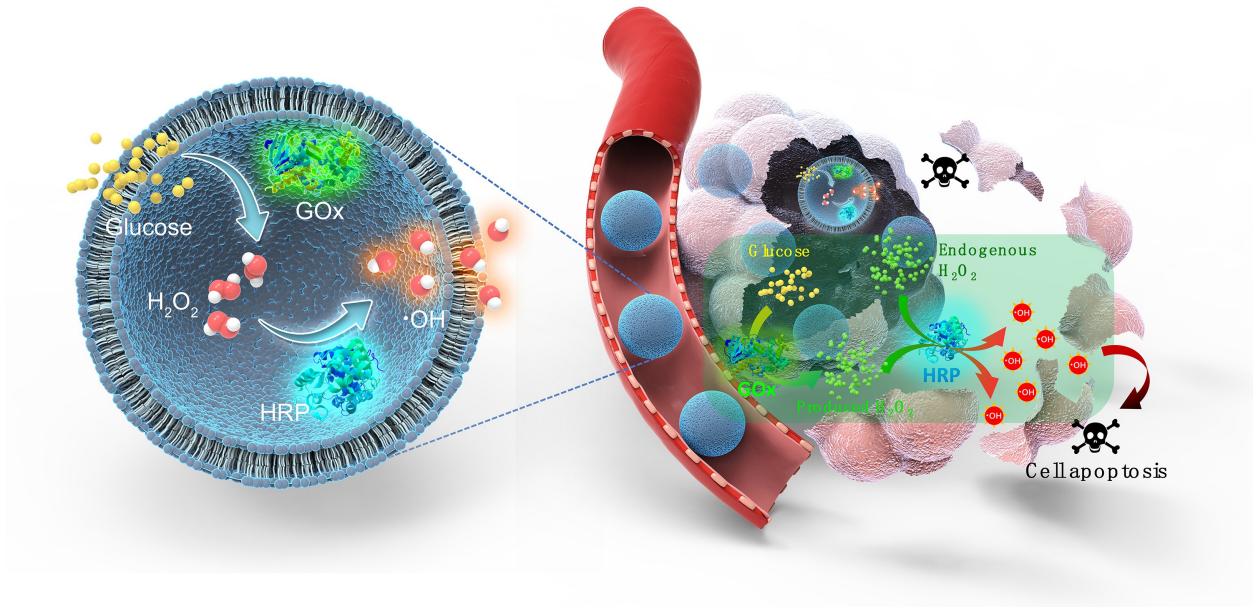

Scheme 1. Scheme of composition and tandem reaction of liposomal nanoreactors (left) and mechanism of tandem reaction-based antitumor therapy (right).

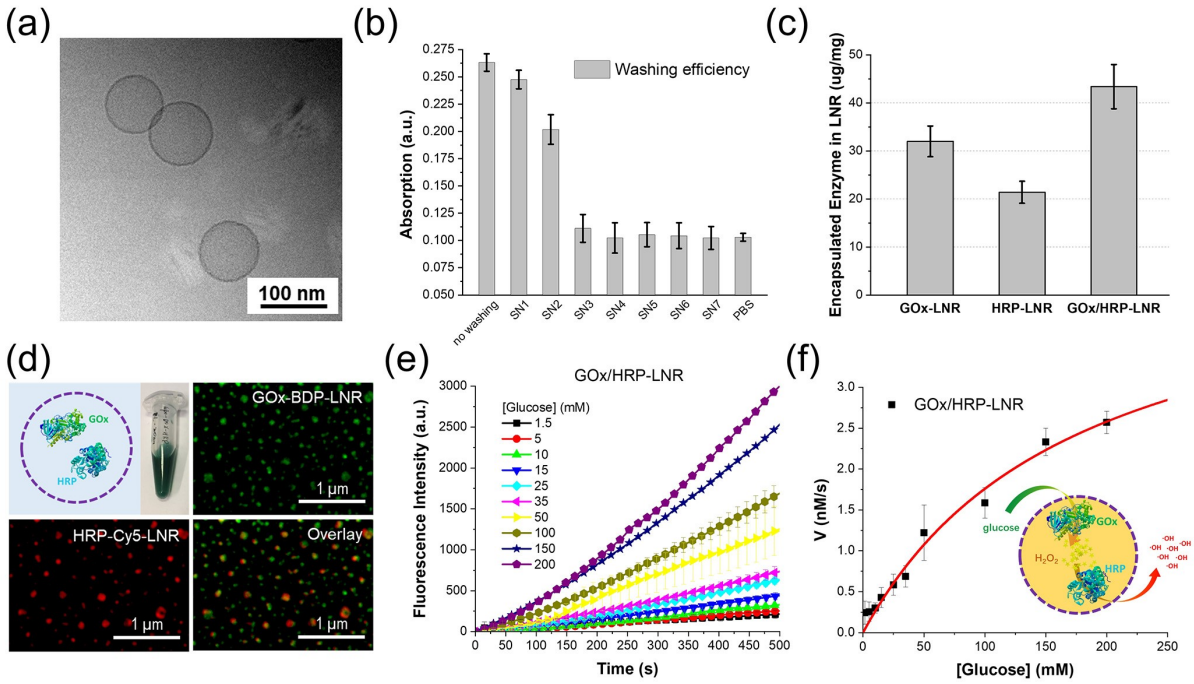

Figure 1. (a) Cryo-TEM image of liposomes. (b) Washing efficiency for removing non-encapsulated enzymes. SN: supernatant obtained from centrifugation. (c) Loading enzyme concentration in LNRs quantified by BCA assay. (d) CLSM images of BODIPY FL-labeled GOx (GOx-BDP) and Cy5-labeled HRP (HRP-Cy5) in the liposomes. (e) Reaction kinetics of GOx/HRP-LNRs with different glucose concentrations. (f) Michaelis–Menten kinetics of cascade reactions by GOx/HRP-LNRs. Data were given as the mean ± SD ($n = 3$).

Table 1: Hydrodynamic radius (R_h) and zeta potential of LNRs loaded with/without different enzymes.

Sample name	Composition	R_h (nm)	PDI	Zeta potential (mV)
Empty-LNRs	Liposome	105	0.13	−30 ± 7
GOx-LNRs	Liposome + GOx	169	0.14	−20 ± 5
HRP-LNRs	Liposome + HRP	161	0.09	−30 ± 8
GOx/HRP-LNRs	Liposome + GOx + HRP	232	0.25	−26 ± 5

GOx or HRP loading alone, while the increase in R_h of GOx/HRP-LNRs was almost double that of single enzyme loading (≈127 nm), indicating that the hydrodynamic radius of LNRs depended on their loading status. In contrast, the zeta potential of LNRs did not change significantly with enzyme addition (stabilized between −20 and −30 mV), indicating good stability of LNRs. To ensure firm entrapping of the enzymes in the aqueous core of LNRs, further purification was performed for enzyme-loaded LNRs. When the number of purification step reached four, the free enzyme concentration in the supernatant hardly changed, meaning that the remaining enzymes were almost wrapped in the LNRs (Figure 1b). The concentration of LNRs in final solutions was adjusted to 1 mg/mL. Correspondingly, the enzyme concentration in samples of GOx-LNRs, HRP-LNRs, and GOx/HRP-LNRs were 32 μg/mL (GOx), 21 μg/mL (HRP), and 43 μg/mL (GOx + HRP), respectively (Figure 1c). To further confirm that both enzymes were co-loaded in the same liposome, GOx and HRP were separately labelled with fluorophore BODIPY FL and Cy5. As shown in Figure 1d, overlap of fluorescent signals from both labelled enzymes was observed, confirming their co-encapsulation. In addition, the negligible change of nanoreactors size with time indicated the good stability of LNRs (Figure S1).

Enzymatic activity of GOx, HRP, and GOx/HRP in LNRs was measured using Amplex™ red fluorescence assay. Reaction kinetics of LNRs were fitted to the Michaelis–Menten model. Kinetic parameters including maximum reaction rate (V_{max}), Michaelis constant (K_M), turnover number (k_{cat}), and catalytic efficiency (k_{cat}/K_M) were determined for GOx-LNRs, HRP-LNRs, and GOx/HRP-LNRs (Table S1). For the GOx-HRP cascade reaction, glucose was provided to the system and consumed by GOx to produce H_2O_2, which is then used as reactant by HRP to generate •OH. These radicals can be detected by oxidizing the non-fluorescent probe Amplex™ red to a highly fluorescent molecule, resorufin. Meanwhile, GOx can also produce gluconic acid as a byproduct, which lowers the pH of the system (Figure S2).

We first studied the enzymatic activity of GOx and HRP after encapsulation (Figure S3). Both enzymes remained

active after encapsulation and the reaction substrates (glucose or H_2O_2) could access the enzymes inside the liposomes. The V_{max} of encapsulated GOx was 2.4 nM/s, ca. 10.4 % of the free GOx rate (Table S1). This reduced activity can be attributed to additional diffusion barriers provided by the liposome lipid bilayer, or it might be due to changes in the enzyme's secondary structure during liposome formation. Nonetheless, no significant changes were observed in the Michaelis constant, indicating that despite being entrapped inside the liposome, GOx has a good affinity for its substrate. For HRP, k_{cat} and k_{cat}/K_M were lower in the encapsulated form. We assume that the temporary product accumulation within the confined space due to delayed diffusion resulted in stronger inhibition of HRP, leading to the observed k_{cat}. Subsequently, we studied the kinetics of the GOx-HRP cascade reaction by monitoring changes in resorufin's fluorescence intensity over time (Figure 1e). In comparison to the free GOx sample, which by default includes the presence of free HRP, co-encapsulation of both enzymes in the liposomes effectively induced the cascade reaction. The K_M of GOx/HRP-LNRs was significantly lower after encapsulation, reflecting improved enzyme affinity for the substrate in the co-encapsulated system (Figure 1f). This might be due to the confined environment provided by the liposomes, which allows an increase in the local concentration of the intermediate product H_2O_2, promoting its efficient utilization by the HRP. Consequently, this caused a 4.4-fold increase in the catalytic efficiency of the GOx/HRP-LNRs system compared to the GOx-LNR sample.

Furthermore, we compared the reactions from LNRs and their corresponding final supernatants during purification process. As shown in Figure S4, for all three LNRs (GOx-LNRs, HRP-LNRs, GOx/HRP-LNRs), there were very low fluorescence produced from their supernatants, confirming that non-encapsulated free enzymes were efficiently removed during the purification procedure, and the monitored reactions of LNRs were from the encapsulated enzymes.

Cell Uptake

Effective cellular uptake is the prerequisite for the antitumor effect of nanoreactors. Flow cytometry and confocal laser scanning microscopy (CLSM) were utilized to investigate the cellular uptake of the LNRs using 1,1′-Dioctadecyl-3,3,3′,3′-Tetramethylindodicarbocyanine,4-Chlorobenzenesulfonate Salt (DiD) as a fluorescence marker. As shown in Figure S5, the fluorescence intensity gradually increased, reaching the maximum at 4 h. However, compared with the fluorescence intensity at 4 h, it decreased at 24 h ($p > 0.05$). Additionally, CLSM confirmed maximum LNR uptake by cells at 4 h (Figure S6). These results demonstrated that tumor cells can effectively take up LNRs and reach uptake saturation at 4 h. Therefore, 4 h was chosen as the incubation time for further cell experiments. Subcellular colocalization images indicated that the LNRs accumulated in the lysosomes (Figure S7).

Intracellular Hydroxyl Radical (•OH) Detection

The key to the antitumor effect of nanoreactors is •OH production. The ability of GOx/HRP-LNRs to generate •OH through enzyme cascade reactions was investigated using a hydroxyphenyl fluorescein (HPF) probe. As shown in Figure 2a, no obvious HPF fluorescence signal was observed in the Empty-LNRs and GOx-LNRs, indicating almost no •OH formation. The weak fluorescence signal in the HRP-LNRs group can be attributed to the low H_2O_2 concentration in tumor cells that HRP can use to produce •OH. In contrast, GOx/HRP-LNRs showed a stronger green fluorescence signal ($p < 0.001$, Figure 2a and b), indicating that GOx in the LNRs could produce sufficient H_2O_2 to compensate the deficiency of HRP substrate in the cells.

ROS levels were evaluated using the commercial ROS tracker 2,7-dichlorodihydrofluorescein diacetate (DCFH-DA). The bright green fluorescence of the GOx/HRP-LNRs further confirmed the enhanced intracellular ROS levels compared to the other three groups (Figure 2c). The above

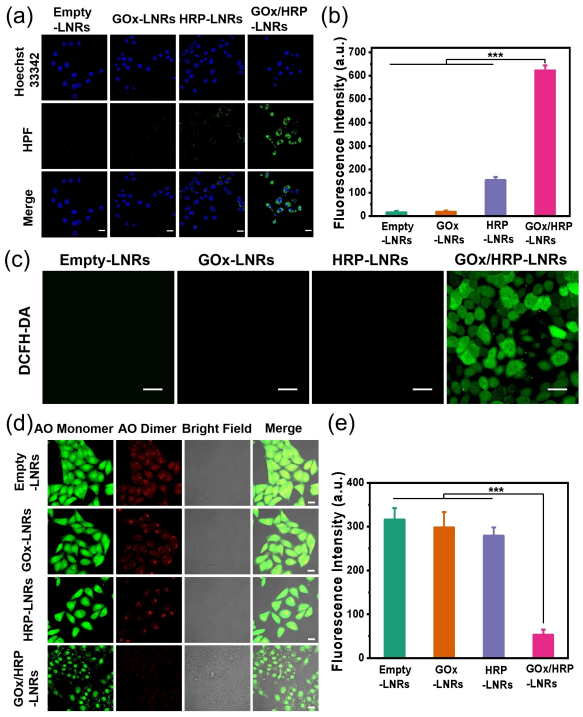

Figure 2. (a) CLSM images of •OH detection in MCF-7 cells using HPF as fluorescence probe (green fluorescence). Scale bars: 20 μm. (b) Average fluorescence intensity of HPF for detecting •OH by CLSM fluorescence intensity analysis. (c) Evaluation of ROS generation in MCF-7 cells by using DCFH-DA after treatment with different LNRs. Scale bars: 30 μm. (d) CLSM images of AO staining for assessing lysosomal integrity in MCF-7 cells after treatment with LNRs. (Green fluorescence: λ_{ex}: 488 nm and λ_{em}: 500–550 nm; Red fluorescence: λ_{ex}: 561 nm and λ_{em}: 600–700 nm). Scale bars: 20 μm. (e) Average fluorescence intensity of AO Red channel for detection of lysosome membrane integrity by CLSM fluorescence intensity analysis. Data were given as the mean ± SD ($n = 3$). Significant difference was defined as * $p < 0.05$, ** $p < 0.01$, and *** $p < 0.001$ determined by Student's t test.

results suggested that GOx/HRP-LNRs could efficiently promote the enzymatic cascade reaction with the help of two enzymes: GOx that catalyzed the generation of H_2O_2 from glucose and HRP that produced •OH with sufficient H_2O_2.

Lysosome Destruction Assay

Lysosomes play important roles in activation of programmed cell death and necrosis;[15] thus, lysosome dysfunction may lead to tumor cell apoptosis. To explore the antitumoral mechanisms of nanoreactors, the effect of •OH produced by GOx/HRP-LNRs by highly efficient enzyme cascade reactions on lysosomes membranes was evaluated by acridine orange (AO) staining. In the complete lysosome, the AO is in a protonated oligomeric form, showing red fluorescence. In the cytoplasm, the AO is deprotonated as a monomer showing green fluorescence. Therefore, the intracellular distribution of AO can be used to evaluate lysosomal membrane integrity. As shown in Figure 2d, bright green and red fluorescence were observed in the cytoplasm and lysosomes in the Empty-LNRs group, respectively, indicating that the LNRs did not induce damage to the lysosomes. Compared with the Empty-LNRs group, the red fluorescence in GOx-LNRs was slightly lower, which may be due to glucose consumption by GOx to produce H_2O_2. Similarly, HRP-LNRs also showed weakened red fluorescence, similar to GOx-LNRs ($p > 0.05$, Figure 2e), indicating that tumor cell lysosomes could also be destructed by HRP-LNRs. HRP-LNRs can produce •OH thanks to endogenous tumor H_2O_2, but its limited concentration leads to insufficient lysosome destructive capacity, which explains the slight decrease in fluorescence in HRP-LNRs. The weakest green fluorescence and almost missing red fluorescence were observed in GOx/HRP-LNRs ($p < 0.001$, Figure 2d and e); the cell shape shrank, indicating that GOx/HRP-LNRs can trigger enzymatic cascade reactions in cells to generate •OH and cause lysosome rupture, inducing cell death. The above results suggested that GOx/HRP-LNRs can not only catalyze glucose depletion in the tumor microenvironment but provide sufficient substrate (H_2O_2) for downstream HRP-catalyzed reactions and produce large amounts of •OH. Meanwhile, we speculated that GOx/HRP-LNRs may kill tumor cells by triggering an enzymatic cascade to induce lysosomal destruction, which may serve as an important experimental basis for GOx/HRP-LNRs to product cytotoxic •OH in vivo.

Cell Cytotoxicity

An MTT assay was used to evaluate GOx/HRP-LNRs cytotoxicity in A549, MCF-7, and 4T1 cells. As shown in Figure 3a, the cell viability of Empty-LNRs was >95%, suggesting that LNRs had little cytotoxicity on tumor cells. Compared with GOx-LNRs, HRP- LNRs showed slight cytotoxicity to A549 cells and 4T1 cells, indicating that the •OH generated by HRP catalysis killed tumor cells. In MCF-7 cells, the cell viability with these two LNRs was close to 100%, which might be due to tumor heterogeneity. Furthermore, the GOx/HRP-LNRs exhibited the strongest dose-dependent cytotoxicity (cell viability was <10% at a LNR concentration of 88 μg/mL), proving that the nanoreactor had high antitumor efficacy. This result was in accordance with the intracellular •OH detection, further proving the hydroxyl radical-based antitumor mechanism of the nanoreactors. Importantly, the nanoreactors exhibited cytotoxicity even under hypoxic conditions (Figure 3b). In fact, inducing apoptosis of cancer cells by ROS often caused by external stimulations. For instance, during conventional photodynamic and sonodynamic therapies, oxygen (O_2) is always converted into singlet oxygen ($^1O_2$) in response to light or ultrasound stimulation.[16] However, the tumor hypoxic conditions, to some extent, limits the $^1O_2$ production (O_2 is converted to $^1O_2$ in a 1:1 ratio). Considering that the nanoreactors produce •OH via intracellular enzymatic reactions, this process with the less oxygen consuming (O_2 is converted to •OH in a 1:2 ratio) and higher toxicity could improve the treatment efficiency under hypoxic conditions.[7a,14a] As expected, although GOx-LNRs and HRP-LNRs induced slight cytotoxicity, GOx/HRP-LNRs had the highest efficient antitumor efficacy on various tumor cells (A549, MCF-7, and 4T1 cells) in hypoxic conditions. The results clearly demonstrated that our nanoreactors could be adapted to tumor hypoxic environments.

Cell Apoptosis

To gain insights into the antitumor mechanism of LNRs, cell apoptosis was detected by flow cytometry, as shown in Figure 3c. Similar to the control group, the survival rate of Empty-LNRs group was above 98%, and negligible apoptotic signals were detected. The GOx-LNRs and HRP-LNRs caused mild early apoptosis (early apoptosis rate: 3.46% for GOx-LNRs and 5.38% for HRP-LNRs) with almost no late apoptosis. While GOx/HRP-LNRs caused strong late apoptosis (late apoptosis rate: 68.2%). Combining the intracellular •OH detection and lysosome destruction assay, we can speculate a latent route related to GOx/HRP-LNRs antitumor mechanisms: ① After the LNRs reach the lysosome, GOx catalyzes H_2O_2 production from glucose; then, HRP further catalyzes H_2O_2 to produce the tumor-killing factor •OH; ② •OH destroys lysosomes, thereby inducing late tumor apoptosis and ultimately killing tumor cells.

Live/Dead Cell Staining

Afterwards, a Calcein-AM/propidium iodide (PI) kit was applied to further assess the therapeutic efficacy of GOx/HRP-LNRs in vitro. Calcein-AM can mark living cells with green fluorescence, and PI can track dead cells with red fluorescence. In Figure 4a, the strongest red fluorescence and the weakest green fluorescence appeared with GOx/HRP-LNRs ($p < 0.001$), which indicated that GOx/HRP-

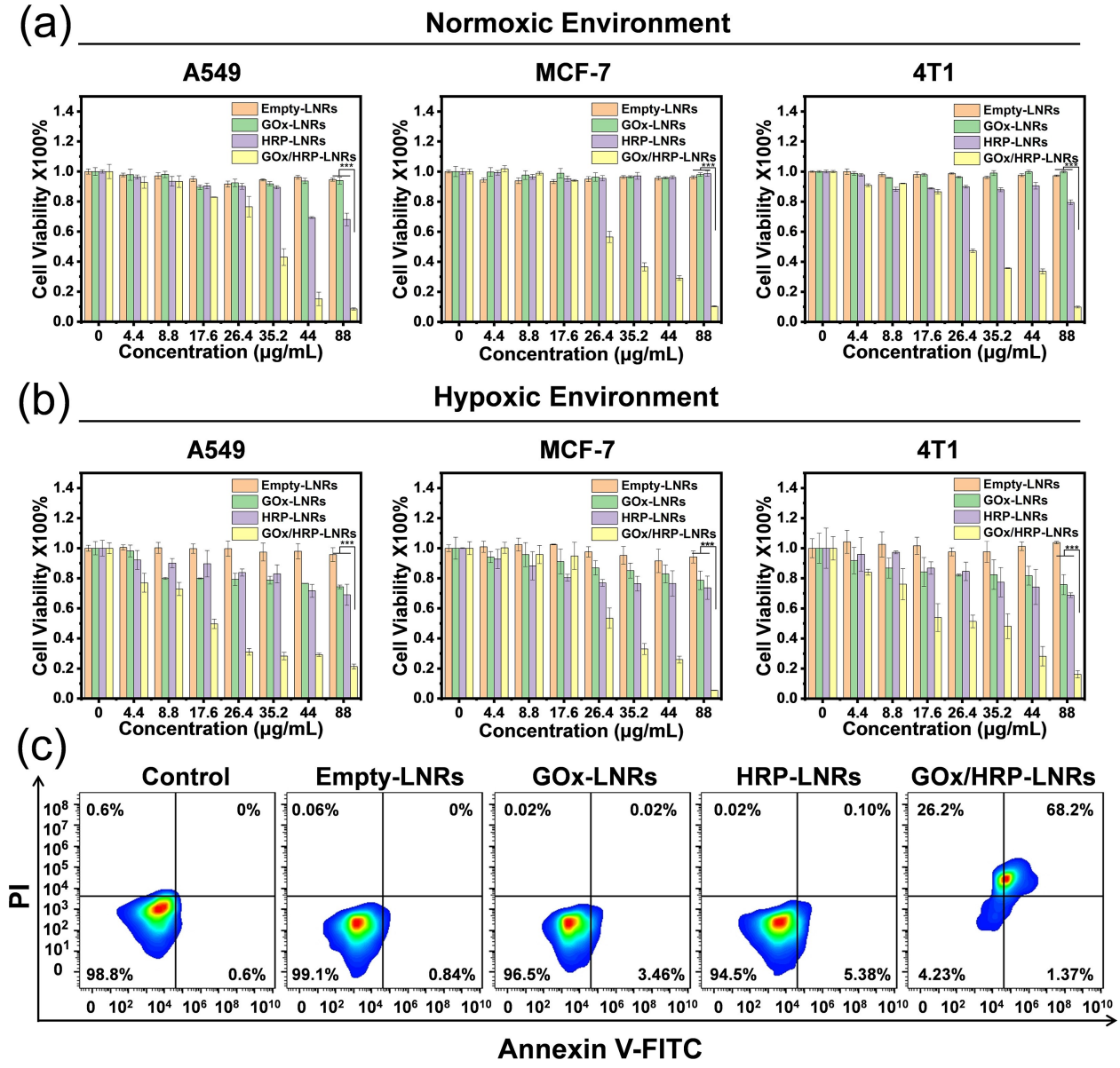

Figure 3. (a) Cell viability of A549, MCF-7, and 4T1 cells treated with different LNR concentrations in normoxic environment. (b) Cell viability of A549, MCF-7, and 4T1 cells treated with different LNRs in hypoxic environment. (c) Cell apoptosis and necrosis analysis shown by flow cytometry. 4T1 cells were stained with Annexin V-FITC/PI kit after incubating cells with PBS, Empty-LNRs, GOx-LNRs, HRP-LNRs, and GOx/HRP-LNRs. Data were given as the mean ± SD ($n = 6$). Significant differences were indicated as $^{*}p < 0.05$, $^{**}p < 0.01$, and $^{***}p < 0.001$ determined by Student's t test.

LNRs could kill tumor cells with high efficiency compared to other LNRs. On the contrary, cells in the Empty-LNRs group were almost stained with green fluorescence ($p < 0.001$, Figure 4a and b). In addition, the red fluorescence intensity of HRP-LNRs was stronger than that of GOx-LNRs ($p < 0.01$, Figure 4a and c), indicating that $^{\bullet}OH$ is the main force killing tumor cells. This result is consistent with the cytotoxicity results, consolidating that GOx/HRP-LNRs exerted antitumor activity via tandem reactions producing $^{\bullet}OH$.

In Vitro and In Vivo Biocompatibility

The biocompatibility of the nanoreactors was evaluated by in vitro hemolysis and in vivo blood index detection, respectively. As shown in Figure S8, after erythrocyte incubated with different concentrations of GOx/HRP-LNRs, hemolysis rate was less than 5%. Moreover, the levels of blood markers and standard blood parameters in each group were in the normal range (Figure S9, S10), indicating that GOx/HRP-LNRs did not cause acute inflammation or organ damage. The above results suggested that GOx/HRP-LNRs have good biocompatibility in vitro and in vivo.

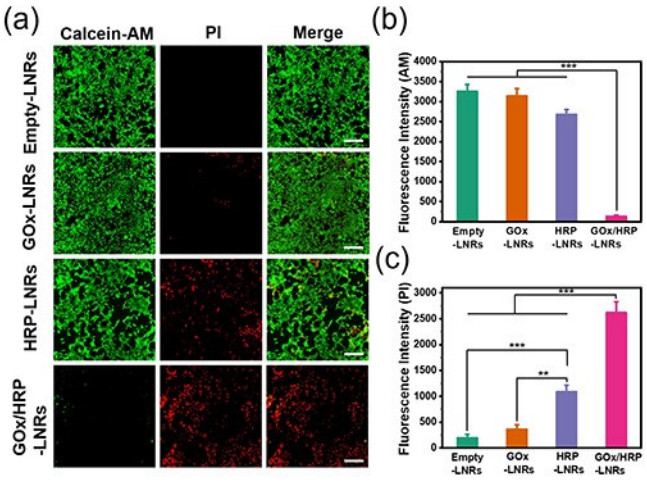

Figure 4. (a) CLSM images of live and dead 4T1 cells stained by Calcein-AM (green channel: λ_{ex}: 488 nm and λ_{em}: 500–580 nm) and PI (red channel: λ_{ex}: 561 nm and λ_{em}: 600–700 nm) after incubation with different LNPs (88 μg/mL). (b) Average fluorescence intensity of live 4T1 cells using Calcein-AM. (c) Average fluorescence intensity of dead 4T1 cells using PI. Scale bars: 150 μm. Data were given as the mean ± SD ($n = 3$). Significant differences were indicated as * $p < 0.05$, ** $p < 0.01$, and *** $p < 0.001$ determined by Student's t test.

In Vivo Assessment of Therapeutic Efficacy

Effective delivery to the tumor site is key for the antitumor efficacy of nanomedicines. Before tail vein injection, we first studied the stability of LNRs in blood. Multiangle DLS results showed that the LNRs were stable in blood without aggregation formed (Figure S14). After systemic administration, time-dependent qualitative biodistribution of DiD-labeled LNRs was monitored in vivo using a non-invasive NIR imaging technique. As shown in Figure 5b, the fluorescence intensity at the tumor site increased after injection, indicating that GOx/HRP-LNRs start to accumulate at the tumor site through the blood circulation. The fluorescence intensity of the tumor site was the strongest, significantly higher than that of other sites at 24 h. The relative fluorescence intensity of the tumor after isolation increased gradually and reached the maximum at 24 h (Figure S11), which was consistent with the results of in vivo experiments. Images of major organs (Figure 5c) at different times after injection of DiD-LNRs further proved the high accumulation capacity of LNRs in the tumor. The percentage of relative fluorescence intensity in major organs (Figure S12) indicated that LNRs were gradually enriched in tumor and metabolized by liver.

The animal administration protocol is shown in Figure 5a. The comparison of tumor volume change and tumor weight of mice treated with different formulations over 18 days is depicted in Figure 5d and e. Compared with normal saline and Empty-LNRs, the tumor volume growth with GOx-LNRs, HRP-LNRs, and GOx/HRP-LNRs was inhibited to varying degrees (Figure 5d). Compared with GOx/HRP-LNRs, GOx-LNRs and HRP-LNRs exhibited relatively weak antitumor activity. In contrast, the tumor volume in mice receiving GOx/HRP-LNRs was significantly smaller. In addition, the tumor weight results displayed a similar trend of tumor suppression as the tumor volume (Figure 5e). The tumor weight of the GOx/HRP-LNRs group was significantly lower than that of the other groups (tumor inhibition rate of 89 %, $p < 0.001$, Figure S13). After treatment, the tumor appearance map (Figure 5g) and anatomical map (Figure 5h) of mice in each treatment group further showed potent GOx/HRP-LNR's antitumor activity. This was in aggreement with the results of in vitro cytotoxicity, which proved that the nanoreactor (GOx/HRP-LNRs) could catalyze an enzymatic cascade to generate $^{\bullet}OH$ to kill tumors in vitro and in vivo.

Furthermore, H&E evaluation was used to assess antitumor efficacy after different treatments. As shown in Figure 5i, tumors in the saline control group or Empty-LNRs group had histologic characteristic indicating rapid tumor growth, including hyperchromatic nuclei, scant cytoplasm, large nucleus, and closely arranged tumor cells. In contrast, the tumors of mice treated with GOx-LNRs, HRP-LNRs, and GOx/HRP-LNRs all exhibited tumor cell shrinkage, large homogeneous red staining of necrotic tissue, and cell separation. This cell apoptotic phenomenon indicated that GOx/HRP-LNR treatment achieved the highest level of tumor necrosis. Next, terminal deoxynucleotidyl transferase-mediated dUTP nick-end labeling (TUNEL) staining was used to evaluate the apoptosis of tumor cells. The apoptosis results (TUNEL fluorescent staining, Figure 5i) showed a higher apoptosis rate in the GOx/HRP-LNRs group (more intensive green fluorescence) than the other groups. These results are highly consistent with those of in vitro apoptosis experiments.

The weight loss of cancer patients is generally considered an indicator of the systemic toxicity of nanomedicines.[17] All mice survived the 18-day monitoring period. Mouse weight fluctuated in all groups, but no significant weight loss was observed (Figure 5f). The toxicity of the different treatments was further estimated via histological analysis of major organs (heart, liver, spleen, lung, and kidney; Figure S15). None of them showed any pathological issue damages or abnormality in all groups. The above results verified the good biocompatibility of the GOx/HRP-LNRs.

Conclusion

We developed liposome-based enzyme nanoreactors for catalytic antitumor therapy. The nanoreactors comprised glucose oxidase and horseradish peroxidase, which consume glucose and produce highly cytotoxic $^{\bullet}OH$ as final product of cascade reactions. Co-compartmentalization of both enzymes in liposomes creates a confined microenvironment that increases local H_2O_2 concentration, hence improving the efficiency of tandem reactions. These liposomal nanoreactors showed good biocompatibility and effectively inhibited tumor growth in vitro and in vivo, showing their potential for the future development of catalytic antitumor nanomedicines. Further efforts on optimizing the ratio of GOx/HRP in liposomes, the scale preparation and improve-

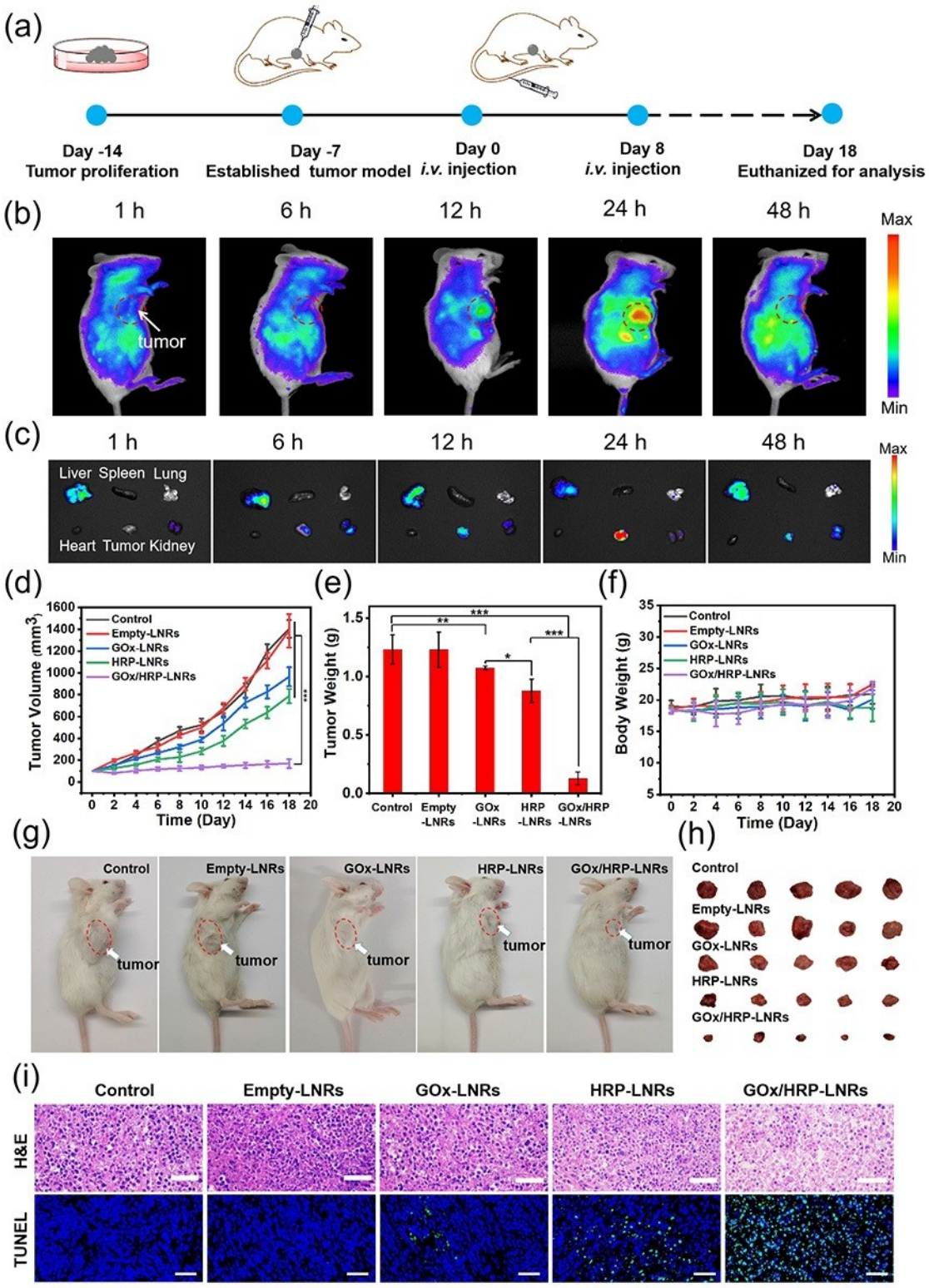

Figure 5. (a) Animal administration protocol. (b) In vivo fluorescence imaging of mice treated with GOx/HRP-LNRs by intravenous injection. (c) Ex vitro fluorescence images of major organs (liver, spleen, lung, heart, tumor and kidney) at different times post intravenous injection of DiD-LNRs. (d) Changes in tumor volume of mice treated with normal saline, Empty-LNRs, GOx-LNRs, HRP-LNRs, and GOx/HRP-LNRs. (e) Average tumor weight in each group after various treatment. (f) Changes of mouse body weight after different treatments. (g) Photo of a mouse in each treatment group after being euthanized. (h) Tumor images of each group after resection. (i) H&E and TUNEL assay analysis of tumor tissues with the different treatments. Scale bar: 50 μm for H&E and TUNEL. Data were given as the mean ± SD ($n = 5$). Significant differences were defined as $^{*}p < 0.05$, $^{**}p < 0.01$, and $^{***}p < 0.001$ determined by Student's t test.

ment of quality control would promote the clinical applications of the liposomal nanoreactors.

Acknowledgements

This work was financially supported by the National Science Foundation of China (22022803, 22078046, 32201149), the Fundamental Research Fundamental Funds for the Central Universities (DUT22LAB601), and the Shandong Provincial Natural Science Fund for Excellent Young Scientists Fund Program (Overseas) (2022HWYQ-063). Open Access funding enabled and organized by Projekt DEAL.

Conflict of Interest

The authors declare no conflict of interest.

Data Availability Statement

The data that support the findings of this study are available from the corresponding author upon reasonable request.

Keywords: Anticancer Therapy · Biomimetic Systems · Cascade Reactions · Catalytic Nanomedicines · Liposomes

[1] a) M. B. Quin, K. K. Wallin, G. Zhang, C. Schmidt-Dannert, *Org. Biomol. Chem.* **2017**, *15*, 4260–4271; b) Q. Qu, X. Zhang, A. Yang, J. Wang, W. Cheng, A. Zhou, Y. Deng, R. Xiong, C. Huang, *J. Colloid Interface Sci.* **2022**, *626*, 768–774; c) E. T. Hwang, S. Lee, *ACS Catal.* **2019**, *9*, 4402–4425; d) Y. Xu, J. Fei, G. Li, T. Yuan, X. Xu, J. Li, *Angew. Chem. Int. Ed.* **2019**, *58*, 5572–5576; e) T. Man, C. Xu, X. Y. Liu, D. Li, C. K. Tsung, H. Pei, Y. Wan, L. Li, *Nat. Commun.* **2022**, *13*, 305.

[2] a) H. C. Kistler, K. Broz, *Front. Microbiol.* **2015**, *6*, https://doi.org/10.3389/fmicb.2015.00068; b) J. Flechsler, T. Heimerl, H. Huber, R. Rachel, I. A. Berg, *Proc. Natl. Acad. Sci. USA* **2021**, *118*, e2022114118.

[3] a) A. E. Engelhart, K. P. Adamala, J. W. Szostak, *Nat. Chem.* **2016**, *8*, 448–453; b) W.-H. Chen, M. Vázquez-González, A. Zoabi, R. Abu-Reziq, I. Willner, *Nat. Catal.* **2018**, *1*, 689–695; c) Z. Zhao, J. Fu, S. Dhakal, A. Johnson-Buck, M. Liu, T. Zhang, N. W. Woodbury, Y. Liu, N. G. Walter, H. Yan, *Nat. Commun.* **2016**, *7*, 10619.

[4] a) H. Tan, S. Guo, N. D. Dinh, R. Luo, L. Jin, C. H. Chen, *Nat. Commun.* **2017**, *8*, 663; b) M. Godoy-Gallardo, C. Labay, V. D. Trikalitis, P. J. Kempen, J. B. Larsen, T. L. Andresen, L. Hosta-Rigau, *ACS Appl. Mater. Interfaces* **2017**, *9*, 15907–15921; c) M. Marguet, C. Bonduelle, S. Lecommandoux, *Chem. Soc. Rev.* **2013**, *42*, 512–529.

[5] a) Z. Chen, F. Hu, Z. Lin, J. Hu, R. Shen, Y. Lin, X. Y. Liu, *Small Sci.* **2021**, *1*, 2000049; b) Z.-L. Li, H. Wu, J.-Q. Zhu, L.-Y. Sun, X.-M. Tong, D.-S. Huang, T. Yang, *Small Sci.* **2022**, *2*, 2200024; c) X. Liu, P. Formanek, B. Voit, D. Appelhans, *Angew. Chem. Int. Ed.* **2017**, *56*, 16233–16238; d) R. J. Peters, M. Marguet, S. Marais, M. W. Fraaije, J. C. van Hest, S. Lecommandoux, *Angew. Chem. Int. Ed.* **2014**, *53*, 146–150; e) Z. Li, Y. Zhang, Y. Su, P. Ouyang, J. Ge, Z. Liu, *Chem. Commun.* **2014**, *50*, 12465–12468; f) Y. Elani, R. V. Law, O. Ces, *Nat. Commun.* **2014**, *5*, 5305.

[6] a) A. Belluati, I. Craciun, C. E. Meyer, S. Rigo, C. G. Palivan, *Curr. Opin. Biotechnol.* **2019**, *60*, 53–62; b) S. M. Jo, F. R. Wurm, K. Landfester, *Nano Lett.* **2020**, *20*, 526–533.

[7] a) S. Jiang, L. Caire da Silva, T. Ivanov, M. Mottola, K. Landfester, *Angew. Chem. Int. Ed.* **2022**, *61*, e202113784; b) S. M. Jo, S. Jiang, R. Graf, F. R. Wurm, K. Landfester, *Nanoscale* **2020**, *12*, 24266–24272.

[8] a) Y. Zhang, B. Y. Hsu, C. Ren, X. Li, J. Wang, *Chem. Soc. Rev.* **2015**, *44*, 315–335; b) K. An, T. Hyeon, *Nano Today* **2009**, *4*, 359–373.

[9] a) W. Ke, J. Li, F. Mohammed, Y. Wang, K. Tou, X. Liu, P. Wen, H. Kinoh, Y. Anraku, H. Chen, K. Kataoka, Z. Ge, *ACS Nano* **2019**, *13*, 2357–2369; b) H. Gumz, S. Boye, B. Iyisan, V. Kronert, P. Formanek, B. Voit, A. Lederer, D. Appelhans, *Adv. Sci.* **2019**, *6*, 1801299.

[10] a) F. Golombek, K. Castiglione, *Biotechnol. J.* **2020**, *15*, 1900561; b) F. Huo, S. Li, Q. Li, Y. Qu, W. Zhang, *Macromolecules* **2014**, *47*, 2340–2349.

[11] a) A. K. Pearce, R. K. O'Reilly, *Biomacromolecules* **2021**, *22*, 4459–4469; b) J. M. Fishman, D. B. Zwick, A. G. Kruger, L. L. Kiessling, *Biomacromolecules* **2019**, *20*, 1018–1027.

[12] a) P. Lefrançois, B. Goudeau, S. Arbault, *Analyst* **2020**, *145*, 7922–7931; b) Y. Zheng, T. Wegner, D. Di Iorio, M. Pierau, F. Glorius, S. V. Wegner, *ACS Chem. Biol.* **2023**, *18*, 1435–1443; c) Y. Zhang, Y. Chen, X. Yang, X. He, M. Li, S. Liu, K. Wang, J. Liu, S. Mann, *J. Am. Chem. Soc.* **2021**, *143*, 2866–2874.

[13] A. Samad, Y. Sultana, M. Aqil, *Curr. Drug Delivery* **2007**, *4*, 297–305.

[14] a) J. Bai, C. Peng, L. Guo, M. Zhou, *ACS Biomater. Sci. Eng.* **2019**, *5*, 6207–6215; b) G. Zhou, M. Li, *Adv. Mater.* **2022**, *34*, 2200871; c) X. He, Y. Hao, B. Chu, Y. Yang, A. Sun, K. Shi, C. Yang, K. Zhou, Y. Qu, H. Li, Z. Qian, *Nano Today* **2021**, *39*, 101174.

[15] a) F. Zhang, Y. Hou, M. Zhu, B. Deng, M. Zhao, X. Zhu, Y. Sun, D. Chen, C. Jiang, L. Wang, C. Chen, H. Chen, H. Chen, H. Zheng, W. Li, *Adv. Sci.* **2021**, *8*, 2102666; b) A. Alu, X. Han, X. Ma, M. Wu, Y. Wei, X. Wei, *Acta Pharm. Sin. B* **2020**, *10*, 1880–1903.

[16] a) X. Xia, R. Wang, Y. Hu, W. Liu, T. Liu, W. Sun, J. Fan, X. Peng, *Front. Chem.* **2021**, *9*, 701771; b) F. Xu, H. Ge, N. Xu, C. Yang, Q. Yao, S. Long, W. Sun, J. Fan, X. Xu, X. Peng, *Sci. China Chem.* **2021**, *64*, 488–498.

[17] a) M. He, G. He, P. Wang, S. Jiang, Z. Jiao, D. Xi, P. Miao, X. Leng, Z. Wei, Y. Li, Y. Yang, R. Wang, J. Du, J. Fan, W. Sun, X. Peng, *Adv. Sci.* **2021**, *8*, 2103334; b) W. Jiang, Y. Wang, J. A. Wargo, F. F. Lang, B. Y. S. Kim, *Nat. Nanotechnol.* **2021**, *16*, 6–15; c) H. Wang, L. Zhou, K. Xie, J. Wu, P. Song, H. Xie, L. Zhou, J. Liu, X. Xu, Y. Shen, S. Zheng, *Theranostics* **2018**, *8*, 3949–3963; d) D. Xi, N. Xu, X. Xia, C. Shi, X. Li, D. Wang, S. Long, J. Fan, W. Sun, X. Peng, *Adv. Mater.* **2022**, *34*, 2106797; e) G. Yang, S. Z. F. Phua, W. Q. Lim, R. Zhang, L. Feng, G. Liu, H. Wu, A. K. Bindra, D. Jana, Z. Liu, Y. Zhao, *Adv. Mater.* **2019**, *31*, 1901513.

Manuscript received: June 21, 2023
Accepted manuscript online: July 26, 2023
Version of record online: September 25, 2023